Effect of Surface Charges on the Rates of Intermolecular Electron-Transfer between de Novo Designed Metalloproteins†

Anna Y. Kornilova,‡,§ James F. Wishart,|| and Michael Y. Ogawa*,‡

Department of Chemistry and Center for Photochemical Sciences, Bowling Green State University, Bowling Green, Ohio 43403, and Chemistry Department, Brookhaven National Laboratory, Upton, New York 11973

Received June 5, 2001; Revised Manuscript Received August 3, 2001

ABSTRACT: A de novo designed coiled-coil metalloprotein was prepared that uses electrostatic interactions to control both its conformational and bimolecular electron-transfer properties. The title protein exists as a coiled-coil heterodimer of the [Ru(trpy)(bpy)-KK(37-mer)] and [Ru$(NH_3)_5$-EE(37-mer)] polypeptides which is formed by interhelix electrostatic attractions. Circular dichroism studies show that the electrostatic heterodimer has $K_d = 0.19 \pm 0.03$ μM and is 96% helical at high concentrations. Intercomplex electron-transfer reactions were studied that involve the [Ru$(NH_3)_5$-H21]$^{2+}$ electron-donor and the [Ru(trpy)(bpy)-H21]$^{3+}$ electron-acceptor belonging to different electrostatic dimers. An important feature of the designed metalloprotein is its two cationic redox centers embedded within protein surfaces having opposite charge. Thus, the $Ru^{II}(NH_3)_5$-H21 site was placed on the surface of one chain of the coiled-coil which was made to be positively charged, and the Ru^{III}(trpy)(bpy)-H21 site was placed on the surface of the other chain which was negatively charged. The rates of intermolecular electron-transfer increased from $(1.9 \pm 0.4) \times 10^7$ M^{-1} s^{-1} to $(3.7 \pm 0.5) \times 10^7$ M^{-1} s^{-1} as the ionic strength was increased from 0.01 to 0.20 M. This indicates that the electrostatic repulsion between the ruthenium centers dominates the kinetics of these reactions. However, the presence of the oppositely charged protein surfaces in the coiled-coils creates an electrostatic recognition domain that substantially ameliorates the effects of this repulsion.

Recent progress in the field of de novo protein design has advanced our understanding of how particular protein structures can be formed from certain amino acid sequences. Several important examples now exist of amino acid sequences that were designed to self-assemble into such important conformations as α-helical bundles (*1*−*4*) and *β*-pleated sheets (*5*−*7*). More recently, inorganic cofactors have begun to be incorporated into such synthetic proteins to produce analogues of zinc finger peptides (*8*−*10*), iron−sulfur proteins (*11*), heme proteins (*12*, *13*), hydrolytic nucleases (*14*), and other types of metalloproteins (*15*).

Among the most well-studied class of de novo designed proteins are the synthetic, two-stranded α-helical coiled-coils that can be described as an intertwining of two α-helices that forms a left-handed supercoil. This motif comprises an important noncovalent dimerization domain found in many natural proteins. Seminal work by Hodges and co-workers (*3*) has shown that polypeptides constructed from amino acid sequences having a 4-3 hydrophobic repeat can spontaneously self-assemble into two-stranded coiled-coils that can be further stabilized by the formation of interhelix salt bridges. In general, these structures are prepared from peptide sequences that are based on a seven residue heptad repeat, $(abcdefg)_n$, in which positions *a* and *d* are occupied by hydrophobic amino acids, positions *b*, *c*, and *f* are occupied by hydrophilic residues, and positions *e* and *g* contain oppositely charged residues which form stabilizing interchain salt bridges. The sequence can be designed to provide a specific pattern of salt bridges to enforce a parallel, in-register alignment of the α-helices. Our group has recently used this design to prepare a synthetic metalloprotein in which a long-range electron-transfer reaction occurs across a well-defined, yet noncovalent peptide−peptide interface (*16*). In that work, a 30-mer polypeptide was designed using the above principles but was modified to incorporate a single histidine residue at position 21, which is the most highly solvent-exposed position of the third heptad repeat. This modification, called H21(30-mer), provided a convenient coordination site for inorganic redox centers through treatment with either [Ru$(NH_3)_5(OH_2)]^{2+}$ or [Ru(trpy)(bpy)$(OH_2)]^{2+}$.[1] A variety of physicochemical techniques were used to determine that both the apo and metalated versions of the protein existed as parallel, two-stranded coiled-coils. The desired ET heterodimer was then prepared in a statistical distribution with the parent metallo-homodimers. Oxidative pulse radiolysis experiments were performed to observe electron-transfer reactions occurring from the $Ru^{II}(NH_3)_5$-H21 donor to the

† This work was supported by the National Institutes of Health Grant GM 61171 and the Petroleum Research Fund grant 34901-AC (MYO). The work at BNL was performed under U.S. Department of Energy, Office of Basic Energy Sciences contract DE-AC02-98CH10886 (JFW). A.Y.K. acknowledges predoctoral support from the Harold and Helen McMaster Foundation.

* To whom correspondence should be addressed. Phone: (419) 372-2809; fax: (419) 372-9809; e-mail: mogawa@bgnet.bgsu.edu.

‡ Bowling Green State University.

|| Brookhaven National Laboratory.

§ Current address: Center for Neurologic Diseases, Brigham and Women's Hospital and Harvard Medical School, 77 Avenue Louis Pasteur, H. I. M. 626, Boston, MA 02115.

[1] Abbreviations: trpy, 2,2′:6′,2″-terpyridine; bpy, 2,2′-bipyridine; k_{et}, electron-transfer rate constant; NMP, *N*-methylpyrrolidone; HBTU, 2-(1H-benzotriazol-1-yl)-1,1,3,3-tetramethyluronium hexafluorophosphate; HOBT, 1-hydroxybenzotriazole; DIEA, *N*,*N*-diisopropylethylamine; DMF, *N*,*N*-dimethylformamide; HTFA, trifluoroacetic acid; HPLC, high performance liquid chromatography; UV−Vis, ultraviolet−visible.

10.1021/bi011156u CCC: $20.00
Published on Web 09/11/2001

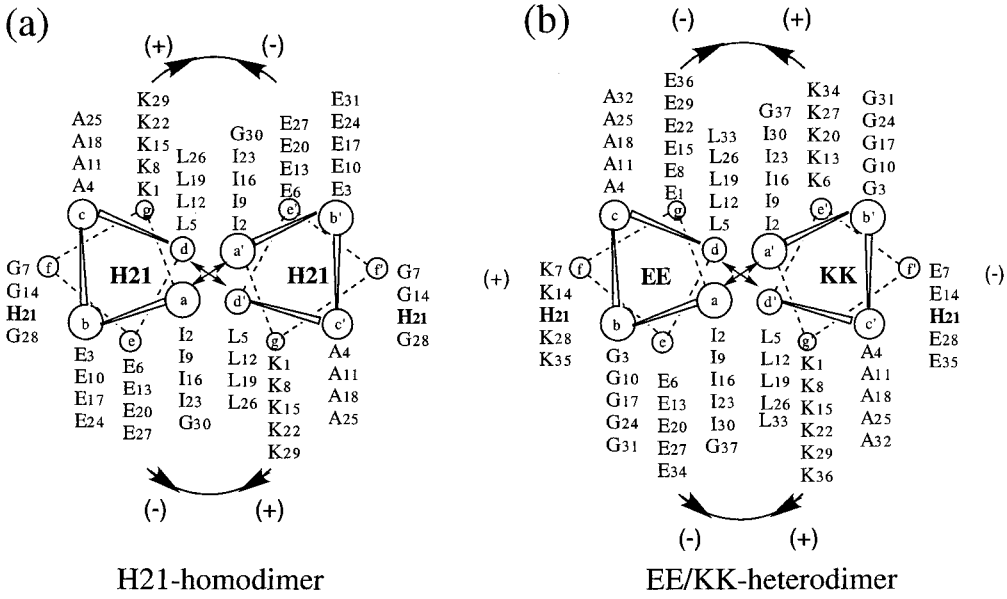

FIGURE 1: Helical wheel representations of the amino acid sequences of the (a) H21(30-mer) homodimer and (b) EE(37-mer)/KK(37-mer) electrostatic heterodimer. The arrows indicate the interchain electrostatic interactions.

Ru^{III}(trpy)(bpy)-H21′ acceptor located ca. 24 Å away across the noncovalent peptide interface with a measured rate constant of $k_{et} = 380 \pm 80\ s^{-1}$.

In this paper, we continue our investigation of the electron-transfer properties of synthetic coiled-coils by using electrostatic interactions to (a) produce an exclusive population of metallo-heterodimers in solution by following previously established design principles (*17*, *18*), and (b) modulate the rates of *inter*-molecular electron-transfer reactions occurring between discrete metalloproteins. Studies of such bimolecular ET reactions will add to our understanding of how electrostatic protein−protein interactions can be used to tune the redox activity of inorganic cofactors for the future design of de novo metalloenzymes. In the current work, two different 37-mer polypeptides were prepared having different electrostatic properties. One peptide, EE(37-mer), has only negatively charged glutamic acid residues occupying its salt-bridging positions (*e* and *g* of the heptad repeat) and the other, KK(37-mer), has only positively charged lysine residues located at these positions. An additional feature of these electrostatic EE(37-mer) and KK(37-mer) polypeptides is that they have oppositely charged surfaces upon which their metal-binding histidine residues are placed. Thus, the EE(37-mer) has a positively charged surface upon which a $Ru(NH_3)_5$- site is attached, and the KK(37-mer) has a negatively charged surface where a Ru(trpy)(bpy)- site is coordinated (Figure 1). The conformational properties and intermolecular electron-transfer properties of the resulting electrostatic heterodimers will be discussed.

EXPERIMENTAL PROCEDURES

Materials. The Fmoc-protected L-amino acid derivatives, *N*-methylpyrrolidone, 2-(1H-benzotriazol-1-yl)-1,1,2,2-tetramethyluronium hexafluorophosphate, piperidine, and hydroxybenzotriazole were purchased from Peptides International, Inc. (Louisville, KY) and PE Biosystems (Foster City, CA). Dichloromethane, and trifluoroacetic acid were obtained from Fisher Scientific (Pittsburgh, PA). Anisole was obtained from Aldrich Chemicals (Milwaukee, WI). All chemicals and solvents were used as received without further purification.

General Methods. Reversed-phase HPLC analyses were performed on either an Agilent Technologies semipreparative (9.4 × 250 mm) or preparative (21.2 × 250 mm) Zorbax 300SB-C18 column. A two-pump system (Waters model 515) equipped with a Waters model 994 diode array detector/spectrophotometer having a 1 cm cell path length was used. For preparative separations, the monitoring wavelengths were set to the tails of the absorption bands of the desired compounds. The purity of the resulting samples were subsequently verified by analytical HPLC runs from which the full UV−Vis spectra could be obtained. Gel filtration was carried out on low-pressure gravity columns packed with Bio-Gel P-2 resin (Bio-Rad Laboratories, Hercules, CA). UV−Vis spectra of the purified compounds were recorded on a Hewlett-Packard model 8452A diode array spectrophotometer. MALDI-TOF mass spectral data were obtained at the Mass Spectrometry Laboratory of the University of Illinois (Urbana-Champaign, Illinois). Cyclic voltammetry was conducted on a BAS 100W Electrochemical Analyzer using a small volume (200 μL) sample cell equipped with a platinum working electrode, a platinum wire auxiliary electrode, and a $Ag/AgNO_3$ reference electrode.

Peptide Synthesis and Purification. Two peptides, having sequences Ac-K(IGALKEK)$_2$-(IGALKHK)-(IGALKEK)$_2$G-amide (denoted as KK(37-mer)), and Ac-E(IGALEKE)$_2$-(IGALEHE)-(IGALEKE)$_2$G-amide (denoted as EE(37-mer)), were synthesized on an PE Biosystems model 433A peptide synthesizer (Forrest City, CA) using the fluorenylmethoxycarbonyl N-terminal protection strategy and the manufacturer's Fmoc-amide resin. Activation was achieved using HBTU and HOBT. Prior to cleavage from the resin, the peptides were *N*-acetylated using a capping solution containing 0.5 M acetic anhydride, 0.125 M DIEA, and 0.015 M HOBT in DMF. The peptides were cleaved from the resin by reaction with HTFA (88% (v/v)), containing phenol (5% (v/v)), triisopropylsilane (2% (v/v)), and water (5% (v/v)), for 2 h. The crude peptides were then precipitated in cold diethyl ether, collected by vacuum filtration, and dried under vacuum. Purification was achieved by either preparative or semipreparative reversed-phase HPLC using a linear AB gradient of 1% (v/v) A/min with a flow rate of 2 mL/min in which solvent A was 0.1% (v/v) trifluoroacetic acid in acetonitrile and solvent B was 0.1% (v/v) trifluoroacetic acid in water. The EE(37-mer) peptides was additionally purified

using a similar gradient in which solvent A was 30% (v/v) of 10 mM ammonia acetate in acetonitrile, and solvent B was 10 mM ammonia acetate. The collected peptides were then lyophilized and analyzed by MALDI-TOF MS (KK(37-mer): *m*/*z* obsd: 3751.9, calcd: 3751.8; EE(37-mer): *m*/*z* obsd: 3758.5, calcd: 3758.0).

Synthesis of Ru(trpy)(bpy)-KK(37mer). In a typical preparation, a 10 mg sample of the KK(37-mer) peptide dissolved in 2 mL of argon-purged 100 mM phosphate buffer (pH 7.0) was added to a concentrated (8−10 mM) solution of [Ru(trpy)(bpy)Cl]Cl (*19*−*21*) dissolved in water. The pH of the reaction mixture was then adjusted to 7.7−7.8. The reaction was allowed to stir under reduced light for 5−7 days at 30−35 °C. The progress of the reaction was monitored by HPLC which showed the growth of a well-resolved peak corresponding to a metalated product, which appeared before the apopeptide. After the reaction was complete, the solution was concentrated to a small volume by rotary evaporation and passed through a gel filtration column equilibrated with water. The metallopeptide solution was then concentrated to near dryness and then lyophilized.

Synthesis of Ru(NH3)5-EE(37mer). In a typical preparation, a 15 mg (34 μmol) sample of $[Ru(NH_3)_5Cl](TFA)_2$ was dissolved in 0.5 mL of water, and the resulting solution was purged with argon for 20−30 min to remove oxygen. A piece of zinc amalgam was then placed into the solution and the solution was bubbled with argon for another 20 min. In a separate flask, 10 mg (3 μmol) of the EE(37-mer) peptide was dissolved in 3 mL of argon-saturated 100 mM phosphate buffer (pH 7) and carefully cannulated into the flask containing the ruthenium complex. The reaction mixture was allowed to stir under an argon atmosphere overnight after which it was filtered and injected directly onto the semi-preparative HPLC column. The products were characterized spectroscopically and electrochemically.

Circular Dichroism Measurements. Circular dichroism spectra were measured with an Aviv and Associates model 62DS circular dichroism spectrometer (Lakewood, NJ) equipped with a thermoelectric temperature controller. A rectangular 1 mm path length cell was used. The spectrometer was routinely calibrated with an aqueous solution of (1S)-(+)-10-camphorsulfonic acid. The spectra were obtained as an average of 3−5 scans using a wavelength step of 1 nm. The thermal denaturation results were obtained by measuring the ellipticity at 222 nm as a function of temperature using a six-second thermal equilibration time between data points and a rate of 1 °C per step.

For the pH-dependence studies, CD spectra were recorded for samples of EE(37-mer) and KK(37-mer) dissolved in aqueous solutions in which additions of $HCl_{(aq)}$ and $NaOH_{(aq)}$ were used to adjust the pH within the range of $1 \leq pH \leq 12$. Care was taken to maintain a constant volume for all samples studied. The samples were incubated at the desired pH for at least 1 h before the spectra were obtained.

Quantitation of the CD results was facilitiated by the preparation of a EE(37-mer)-GGY polypeptide in which a tyrosine residue was attached to the C-terminus of the peptide for use as a spectroscopic probe. For the CD binding studies, samples of the electrostatic heterodimer were prepared by mixing stock solutions of the EE(37-mer)-GGY and KK(37-mer) peptides until a maximum ellipticity at 222 nm was obtained to indicate the formation of an equimolar solution of the two peptides, as discussed in the results section. The actual concentration of the EE(37-mer) in these solutions, and thus of the electrostatic heterodimer, was then determined spectroscopically ($\epsilon_{275\ nm} = 1.5 \times 10^3\ M^{-1}\ cm^{-1}$).

Pulse Radiolysis Measurements. Electron pulse-radiolysis transient-absorption experiments were performed using the 2 MeV Van de Graaff accelerator at Brookhaven National Laboratory with a PC-controlled, CAMAC-based control and data acquisition system. The optical detection system consisted of a (pulsed or CW) xenon arc lamp, appropriate long-pass optical filters, quartz radiolysis cells with various path lengths (2.0 cm in this study), a monochromator and photomultiplier tube. Digitizer traces were fit to single or double first-order kinetics by nonlinear least-squares methods. Azide radical, $N_3^{\bullet}$, was produced by the reaction of radiolytically generated hydroxyl radical ($^{\bullet}OH$) with the azide ion present in the N_2O-saturated water.

$$H_2O + 2\ MeV\ e^- \rightarrow e_{aq}^-, OH^{\cdot}, H^{\cdot}, H_2, H_2O_2$$

$$e_{aq}^- + N_2O + H_2O \rightarrow N_2 + OH^{\bullet} + OH^-$$

$$OH^{\cdot} + N_3^- \rightarrow N_3^{\bullet} + OH^-$$

Radiolytic dose levels were calculated for each shot based on the current delivered and a calibration factor obtained from the $(SCN)_2^-$ dosimeter ($G = 6.13$, $\epsilon = 7950$ at 472 nm). The yield of $N_3^{\bullet}$ radicals (G value) was assumed to be 6.0 per 100 eV absorbed. The concentration of $N_3^{\bullet}$ radicals in each shot was 5−15% of the ruthenated peptide concentration.

Solutions for pulse radiolysis were prepared by reducing a stock solution of equal mole quantities of the $[Ru^{II}(trpy)(bpy)$-KK(37-mer)] and $[Ru^{III}(NH_3)_5$-EE(37-mer)] peptides in phosphate buffer of the appropriate ionic strength (pH 7.0) over zinc amalgam under an argon atmosphere. The concentrations of the [Ru(trpy)(bpy)-KK(37-mer)] metallopeptide present in the solution were determined spectroscopically. Measured quantities of the stock solution were then transferred via gastight syringes and diluted to the desired peptide concentration by addition to a N_2O-saturated solution of the appropriate phosphate buffer solution containing 1 mM NaN_3 in the radiolysis cell. Phosphate buffer solutions having ionic strengths within the range of 0.01−0.20 M were prepared according to literature methods (*22*).

The bimolecular ET rate constants were determined by plotting the observed first-order rate constants of the bleach recovery at 490 nm as a function of the initial concentration of $[Ru(NH_3)_5$-EE(37-mer)] peptide present in the sample. It was assumed that all of the ruthenium pentammine sites were completely reduced to the 2+ oxidation state prior to pulse radiolysis experiment. Only data obtained from the first pulse on each sample were analyzed.

RESULTS AND DISCUSSION

Synthesis and Characterization of Peptides EE(37-mer) and KK(37-mer). The peptides EE(37-mer) and KK(37-mer) were designed according to principles developed (*17*, *18*) for the preparation of electrostatic coiled-coil heterodimers.

Ac-**E(**IGAL**EK**E**)**$_2$-(IGAL**E**H**E**)-(IGAL**EK**E**)**$_2$G-amide
EE(37-mer)

Ac-**K(**IGAL**K**E**K**)$_2$-(IGAL**K**H**K**)-(IGAL**K**E**K**)$_2$G-amide
KK(37-mer)

As shown in the wheel diagram depicted in Figure 1, these sequences differ from that of the H21(30-mer) in which the *e* and *g* positions of the sequence were respectively occupied

by glutamic acid and lysine residues to create a pattern of interhelix salt bridges that enforced a parallel arrangement of α-helices. In contrast, the design of electrostatic heterodimers required that negatively charged glutamic acid residues be placed at *all* of the *e* and *g* positions of the EE(37-mer), and positively charged lysine residues be located at *all* of the *e* and *g* positions of the KK(37-mer). To avoid the possible formation of intrachain (i, $i + 3$) lactam bridges in the KK(37-mer) the occupation of the *b* positions in both peptides was changed from glutamic acid to glycine (*23*). Another important feature of these sequences is the presence of charged residues located at the most solvent-exposed positions of the sequence. Thus, the EE(37-mer) has most of its *f* positions occupied by lysine residues and the KK(37-mer) has most of these sites occupied by glutamic acid groups. In addition to increasing the solubility of the peptides, these latter substitutions have the effect of creating oppositely charged surfaces for these peptides upon which a metal-binding histidine residue is placed at position 21 of the sequence.

The EE(37-mer) and KK(37-mer) peptides were prepared by solid-phase methods, purified by reversed-phase HPLC, and analyzed by MALDI-TOF MS. The two metallopeptides [Ru(trpy)(bpy)KK(37-mer)] and [$Ru(NH_3)_5$EE(37-mer)] were prepared by methods previously described for the metalation of the H21(30-mer) (*16*). The UV absorption spectrum of the [Ru(trpy)(bpy)-KK(37-mer)] peptide is identical to that previously reported for [Ru(trpy)(bpy)-H21(30-mer)] (*16*). In addition, differential pulse polarography and cyclic voltammetry show a reversible redox couple for the metallopeptide at $E° = +1.14$ V vs NHE. As with the case of the H21(30-mer) a second redox couple was observed at 0.86 V vs NHE which is assigned to the presence of uncoordinated [Ru(trpy)(bpy)(H_2O)] which is observed as a minor component (<3%) in the HPLC traces of the peptide sample. The [$Ru(NH_3)_5$-EE(37-mer)] peptide was characterized by cyclic voltammetry that showed a single, reversible one-electron reduction at $E° = +0.044$ V vs NHE which is identical to the behavior observed for the metalated H21(30-mer) (*16*).

Circular Dichroism Spectroscopy. Figure 2 shows the circular dichroism (CD) spectra of the EE(37-mer) and KK(37-mer) peptides taken at 298 K as a function of pH. Figure 2a shows that at pH > 6.0, the CD spectrum of EE(37-mer) consists of a shallow minimum at 222 nm, a stronger minimum at 202 nm, and a strong positive signal at <200 nm, which is diagnostic for a random coil conformation. However, as the pH is lowered, the spectra begin to change, and their features indicate the formation of an α-helical structure, with double minima occurring at 222 and 208 nm, and a maximum appearing at lower wavelengths. When the pH is less than 4, the signals at 222 and 208 nm reach their maximum values, and the ratio of $\theta_{222\ nm}/\theta_{207\ nm}$ becomes 1.04 to indicate the formation of the coiled-coil structure (*3*). The appearance of an isodichroic point at 202 nm, demonstrates that a two-state transition occurs between the disordered and ordered conformations. Thus, when dissolved in basic media the glutamic acid side-chains of EE(37-mer) are deprotonated and electrostatic repulsions between the individual peptide strands prevent the formation of the coiled-coil homodimer. However, lowering of the pH eliminates these unfavorable electrostatic interactions and the peptides self-associate into the ordered structure.

Figure 2b shows analogous changes occurring in the CD spectra of KK(37-mer) as function of pH. At pH < 8, the spectra are typical of those seen for random coils. However, as the pH is increased the lysine side-chains become

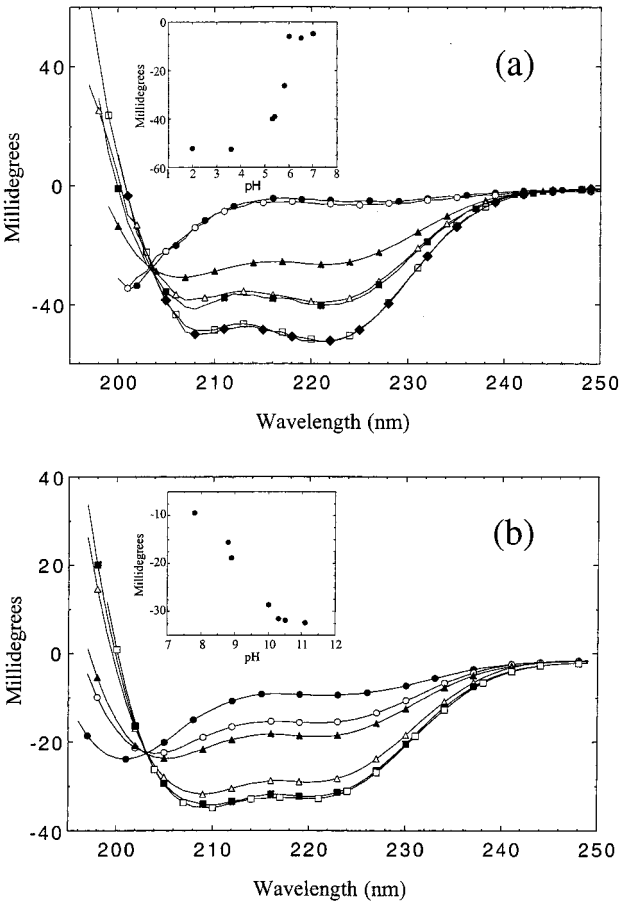

FIGURE 2: Circular dichroism spectra at 298 K of (a) EE(37-mer) at pH 7.0 (●), 6.0 (○), 5.8 (▲), 5.4 (△), 5.3 (■), 3.6 (□), 2.0 (◆). Inset: pH dependence of θ_{222} as a function of pH. (b) KK(37-mer) at pH 7.8 (●), 8.8 (○), 8.9 (▲), 10.0 (△), 10.5 (■), 11.1 (□). Inset: pH dependence of θ_{222} as a function of pH.

deprotonated to produce a transition to the coiled-coil conformation. The data (insets) yield a midpoint at pH 5.7 for the acidic EE(37-mer) peptide and one at pH 9.1 for the basic KK(37-mer).

Figure 3 shows the CD spectra of different mixtures of the EE(37-mer) and KK(37-mer) peptides measured at pH 7, conditions at which the individual peptides do not form coiled-coils by themselves. Figure 3a shows that as the positively charged KK(37-mer) is titrated into a solution of the negatively charged EE(37-mer), the CD spectra begin to change from that of a random coil to that of an α-helical coiled-coil. The minima at 208 and 222 nm grow in intensity until they reach a maximum value when an equimolar mixture of the two peptides is attained. At this point, the ellipticity ratio ($\theta_{222}/\theta_{208}$) reaches a value of 1.06 which indicates the formation of a coiled-coil. The observation of an isodichroic point at 203 nm indicates a two-state, random-coil-to-α-helix transition. Figure 3b shows that similar changes in the CD spectra occur upon the titration of the EE(37-mer) peptide into a solution of the KK(37-mer). These results demonstrate that an equimolar mixture of the EE(37-mer) and KK(37-mer) peptides results in the formation of an electrostatic coiled-coil heterodimer (*3*, *17*, *24*).

The stability of the electrostatic coiled-coil was determined by examining the concentration dependence of θ_{222} measured for an equimolar mixture of the EE(37-mer)-GGY and KK(37-mer) peptides as described in the experimental section. The value of θ_{222} increases with increasing heterodimer concentration and follows eq 1 which describes a

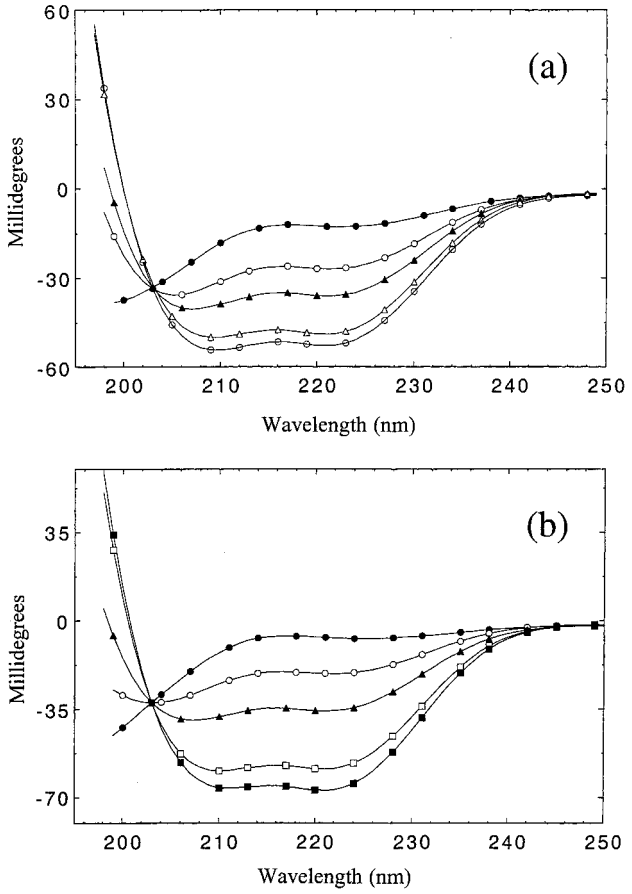

FIGURE 3: Circular dichroism spectra of solutions containing different molar ratios of the EE(37-mer) and KK(37-mer) peptides taken at 298 K in 50 mM phosphate buffer, pH 7 (a) KK:EE = 100:0 (●), 90:10 (○), 80:20 (▲), 60:40 (△), 50:50 (⊖). (b) EE/KK = 100:0 (●), 90:10 (○), 80:20 (▲), 60:40 (□), 50:50 (■). For these experiments, the total peptide concentration was held constant at ca. 80 μM.

two-state monomer−dimer equilibrium. In eq 1,

$$K_d = 2[M_0]\,(1 - \Delta\theta/\Delta\theta_{max})^2/(\Delta\theta/\Delta\theta_{max}) \qquad (1)$$

$[M_0]$ is the total peptide concentration, $\Delta\theta = (\theta_{obs} - \theta_0)$, $\Delta\theta_{max} = (\theta_{max} - \theta_0)$, θ_{max} is the ellipticity of the folded dimer, and θ_0 is the ellipticity of the unfolded monomer usually taken to be 2500 deg cm^2 dmol^{-1}, and all ellipticities are measured at 222 nm (*25*). A nonlinear fit of the data (not shown) yields a value of $K_d = 0.19 \pm 0.03$ μM and $\theta_{max} = -33\,804 \pm 132$ deg cm^2 dmol^{-1}. This value of K_d is an order of magnitude smaller than that measured for the H21(30-mer), which indicates that altering the electrostatic interactions in these systems greatly enhances the stability of the coiled-coil.

The maximum ellipticity determined from the fit to eq 1 can be used to determine the helical content of the heterodimer by comparison to the value predicted for the peptide according to eq 2:

$$X_H^{\infty} = (-37\,400 \text{ deg cm}^2 \text{ dmol}^{-1})(1 - k/n) = -34{,}872 \text{ deg cm}^2 \text{ dmol}^{-1} \qquad (2)$$

where k is a wavelength-dependent constant equal to 2.5 at 222 nm, and n is the number of residues per helix (*26*). This analysis shows that the electrostatic heterodimer has a 96% maximum helicity.

Electron-Transfer Measurements. On the basis of the above results, electron-transfer measurements were performed on solutions containing equimolar samples of the [Ru(trpy)(bpy)KK(37-mer)] and [Ru(NH$_3$)$_5$EE(37-mer)] peptides. Under these conditions, it is believed that the peptides exist exclusively within a population of electrostatic heterodimers since at pH 7 electrostatic repulsions are shown to prevent the formation of homodimers. Oxidative pulse radiolysis techniques were used to measure the kinetics of electron-transfer occurring in these samples according to Scheme 1 in which the radiolytically generated azide radical was used to oxidize either of the two ruthenium centers in the reduced heterodimer to create a nonequilibrium distribution of the two singly oxidized species. Inter- and/or intracomplex electron-transfer brings the system back to redox equilibrium. The kinetic measurements were carried out on solutions containing 5, 10, and 15 μM of the electrostatic heterodimer in phosphate buffer of various ionic strengths. The usable concentration range was limited by the dimer formation equilibrium at the low end and by optical density and signal amplitude at the high end. In addition, at low peptide concentrations, oxidation of the [Ru^{2+}(NH$_3$)$_5$-EE(37-mer)] species was sometimes observed prior to radiolysis, probably due to the introduction of trace amounts of oxygen during sample handling.

The radiolytically initiated electron-transfer processes were monitored at 490 nm, the wavelength at which the largest absorbance change occurs for [Ru$^{2+/3+}$(trpy)(bpy)] redox couple. This wavelength was determined from the difference absorption spectrum obtained during the control experiment involving oxidation of [Ru(trpy)(bpy)KK(37-mer)] with azide radical. Controls were performed on solutions of the [Ru-(trpy)(bpy)KK(37-mer)] peptide alone having concentrations in the range of 5 to 20 μM. In these experiments, a rapid bleach at 490 nm was seen which indicates the formation of [Ru^{III}(trpy)(bpy)KK(37-mer)] species. In the absence of a reductant, the absorption bleach showed evidence of a slow recovery with a rate constant of $k_0 \approx 10^2$ s^{-1}. This behavior is in contrast to that of the corresponding [Ru^{III}(trpy)(bpy)-H21(30-mer)] species which had up to a 100-fold slower recovery rate. Preliminary control experiments suggest that the different behavior of the [Ru^{III}(trpy)(bpy)KK(37-mer)] species may be related to the additional lysine residues present in this peptide.

Scheme 1

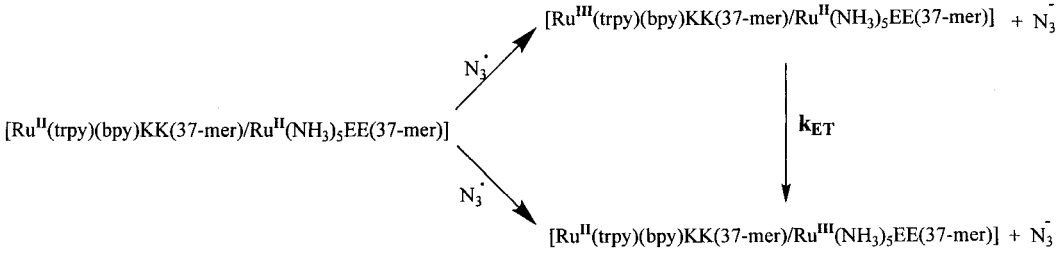

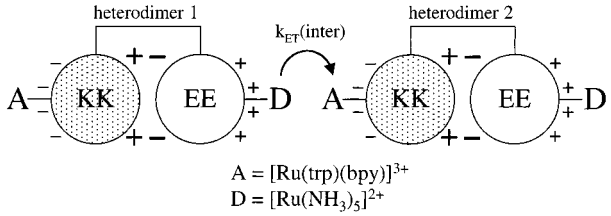

FIGURE 4: Schematic representation of the EE/KK electrostatic heterodimer emphasizing the charges on the solvent-exposed and interfacial regions of the heterodimer.

Table 1: Ionic Strength Dependence of Intermolecular Electron-Transfer Rate Constants

ionic strength (M)	k_{inter} (10^7 M^{-1} s^{-1})
0.01	1.9(4)
0.10	3.2(2)
0.20	3.7(5)

The pulse radiolysis of a 15 μM solution of the electrostatic heterodimer in 50 mM phosphate buffer yields an initial bleach at 490 nm corresponding to the formation of the [Ru^{3+}(trpy)(bpy)KK(37-mer)] species which recovers via first-order kinetics (not shown). The rate constant for this process was seen to vary with the concentration of ET heterodimer within the range of 5 to 15 μM to yield a value of $k_{inter} = 3.2(2) \times 10^7$ M^{-1} s^{-1} for the intermolecular ET reaction occurring between discrete heterodimers. Interestingly, unlike for the related H21(30-mer) system, no evidence could be observed for an intracomplex electron-transfer reaction occurring within the electrostatic heterodimer. This may be due in part to the faster intrinsic decay of the [Ru^{III}-(trpy)(bpy)KK(37-mer)] species which occurs on the same time scale as the previously observed intracomplex electron-transfer reaction. In addition, we note that a principal modification of the EE(37-mer)/KK(37-mer) heterodimer is the different arrangement of interhelix salt-bridges that were used by the H21(30-mer) to ensure the formation of a parallel coiled-coil. These differences will likely affect the conformational properties of the peptide, and it is possible that the electrostatic heterodimer may exist in conformation(s) that would have longer donor−acceptor distances to result in a slower rate of intracomplex electron-transfer.

Ionic Strength Dependence of k_{inter}. An important feature of the ET hetereodimer is that its metal-based electron-donor and acceptor sites were placed within oppositely charged surfaces of the protein (Figure 4). Thus, the ruthenium pentammine electron-donor was attached to the positively charged surface of the EE(37-mer) and the ruthenium polypyridyl electron-acceptor was attached to the negatively charged surface of the KK(37-mer). Upon formation of the electrostatic heterodimer, this situation afforded the possibility that each metalloprotein possessed a set of complementary electrostatic recognition domains that may affect the rates of intermolecular ET occurring between separate dimers. To investigate this hypothesis, ET measurements were performed in phosphate buffers having ionic strengths in the range of 0.01−0.2 M. As shown in Table 1, the resulting bimolecular rate constants increased with increasing ionic strength to indicate that the electrostatic ET effects were dominated by the mutual repulsion of the two positively charged ruthenium centers. These results are consistent with earlier observations that electrostatic interactions involving metalloproteins frequently involve localized charges and not the overall charge of the protein (*27*, *28*).

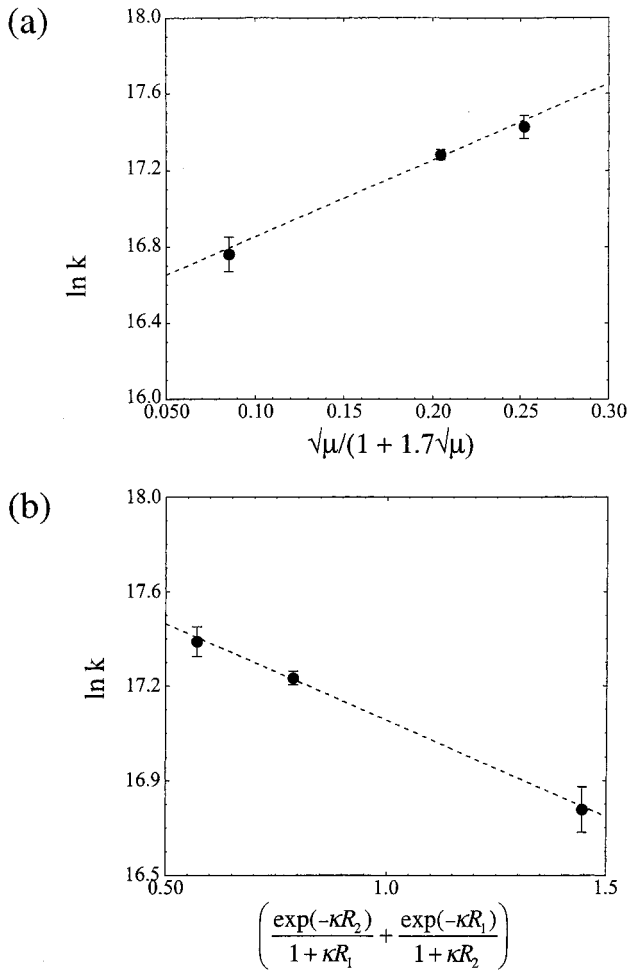

FIGURE 5: Ionic strength dependence of the bimolecular ET rate constants: (a) Fit of the data to the Debye−Huckel expression in eq 3. (b) Fit of the data to eq 4. The observed data are from Table 1.

As a first approach toward understanding how the protein environment of the ET heterodimer can influence the rates of bimolecular electron-transfer, the data in Table 1 were analyzed according eq 3 which results from considering the ionic strength dependence of the activity coefficients of the reactants and transition state in terms of the

$$\ln k = \ln k_0 + \frac{2\alpha Z_1 Z_2 \sqrt{\mu}}{1 + \kappa R_{av}} \qquad (3)$$

Debye−Huckel theory. In eq 3, k is the bimolecular electron-transfer rate constant at ionic strength μ, k_0 is the rate constant at $\mu = 0$, $\alpha = 1.17$ in water, Z_1 and Z_2 are the reactant charges, $\kappa = 0.329\sqrt{\mu}$ Å^{-1}, and R_{av} is the reactant radius which must be identical for each of the two reactants if eq 3 is to obtain (*29*, *30*). In this study, the electron-transfer reaction involves the two solvent-exposed ruthenium centers, and it is assumed that $R_{av} = 5.25$ Å, which is the arithmetic mean of the radii of $Ru(NH_3)_6^{2+}$ ($R_1 = 3.5$ Å) and $Ru(bpy)_3^{3+}$ ($R_2 = 7$ Å) (*31*). Figure 5a shows that the data presented in Table 1 can be accurately described by eq 3, as the plot of ln k vs $\sqrt{\mu}/(1 + 1.7\sqrt{\mu})$ is linear. However, a fit of these data to the equation yields values of $k_0 = 1.4 \times 10^7$ M^{-1} s^{-1} and $Z_1Z_2 = 1.7 \pm 0.3$, of which the latter is significantly smaller than the charge product expected for a cationic electron-donor/acceptor pair having charges of +2 and +3, respectively. It is further noted that this value of Z_1Z_2 is

obtained by using a solvent dielectric constant of 78.5, and therefore represents an upper-limit to apparent charge product. These results suggest that when the $[Ru(NH_3)_5(His)]^{2+}$ electron-donor and the $[Ru(trpy)(bpy)(His)]^{3+}$ electron-acceptor are embedded within the charged protein surfaces of the EE/KK heterodimer, their repulsive interactions are significantly diminished.

A different treatment of the ionic strength dependence of bimolecular ET rate constants is based on the Marcus theory of electron-transfer reactions, but which explicitly considers the Coulombic work terms involved in the formation of the activated complex to produce eq 4 (*29*, *32*).

$$\ln k = \ln k_\infty - 3.576\left(\frac{\exp(-\kappa R_2)}{1+\kappa R_1} + \frac{\exp(-\kappa R_1)}{1+\kappa R_2}\right)\frac{Z_1 Z_2}{R_1 + R_2} \quad (4)$$

In this expression, k_∞ is the bimolecular rate constant at infinite ionic strength, R_1 and R_2 are the radii of the donor and acceptor groups, and the remaining quantities are as defined above for eq 3. Figure 5b shows that eq 4 can also be used to describe the data in Table 1. A fit to the data yields values of $k_\infty = 5.8 \times 10^7\ M^{-1}\ s^{-1}$, and $Z_1Z_2 = 2.3 \pm 0.4$. The value of the ion product determined here is in very close agreement with that obtained from the Debye−Huckel treatment, both of which are less than half the value expected for the free metal complexes. Together, these results demonstrate that electrostatic protein−protein interactions can be used to control the redox activity of inorganic cofactors incorporated into de novo desiged metalloproteins.

ACKNOWLEDGMENT

The authors thank Dr. Norman Sutin for critically reading the manuscript prior to submission.

SUPPORTING INFORMATION AVAILABLE

Plots of k_{obs} vs peptide concentration. This material is available free of charge via the Internet at http://pubs.acs.org.

REFERENCES

1. Hill, R. B., Raleigh, D. P., Lombardi, A., and Degrado, W. F. (2000) *Acc. Chem. Res. 33*, 745−754.
2. Dieckmann, G. R., and DeGrado, W. F. (1997) *Curr. Opin. Struct. Biol. 7*, 486-494.
3. Hodges, R. S. (1996) *Biochem. Cell Biol. 74*, 133−154.
4. Cohen, C., and Parry, D. A. D. (1990) *Proteins 7*, 1−15.
5. Nowick, J. S. (1999) *Acc. Chem. Res. 32*, 287−296.
6. Gellman, S. H. (1998) *Curr. Op. Chem. Biol. 2*, 717−725.
7. Schneider, J. P., and Kelly, J. W. (1995) *Chem. Rev. 95*, 2169−2187.
8. Hori Y, S. K., Okuno Y, Nagaoka M, Futaki S, Sugiura Y. (2000) *J. Am. Chem. Soc. 122*, 7648−7653.
9. Cox, E. H., and McLendon, G. L. (2000) *Curr. Op. Chem. Biol. 4*, 162−165.
10. Imperiali, B., and Ottesen, J. J. (1998) *Biopolymers 47*, 23−29.
11. Mulholland, S. E., Gibney, B. R., Rabanal, F., and Dutton, P. L. (1999) *Biochemistry 38*, 10442−10448.
12. Gibney, B. R., and Dutton, P. L. (2001) *Adv. Inorg. Chem. 51*, 409−455.
13. Shifman, J. M., Gibney, B. R., Sharp, R. E., and Dutton, P. L. (2000) *Biochemistry 39*, 14813−14821.
14. Welch, J. T., Sirish, M., Lindstrom, K. M., and Franklin, S. J. (2001) *Inorg. Chem. 40*, 1982−1984.
15. Xing, G., and DeRose, V. J. (2001) *Curr. Op. Chem. Biol. 5*, 196−200.
16. Kornilova, A. Y., Wishart, J. F., Xiao, W., Lasey, R. C., Fedorova, A., Shin, Y. K., and Ogawa, M. Y. (2000) *J. Am. Chem. Soc. 122*, 7999−8006.
17. Graddis, T. J., Myszka, D. G., and Chaiken, I. M. (1993) *Biochemistry 32*, 12664−12671.
18. Zhou, N. E., Kay, C. M., and Hodges, R. S. (1994) *J. Mol. Biol. 237*, 500−512.
19. Johnson, E. C., Sullivan, B. P., Salmon, D. J., Adeyemi, S. A., and Meyer, T. J. (1978) *Inorg. Chem. 17*, 2211−2215.
20. Sullivan, B. P., Calvert, J. M., and Meyer, T. J. (1980) *Inorg. Chem. 19*, 1404−1407.
21. Ware, D. C., Lay, P. A., and Taube, H. (1986) *Inorg. Synth. 24*, 299−306.
22. *The Chemist's Companion: A Handbook Of Practical Data, Techniques, And References.* (1972) John Wiley and Sons, New York.
23. Houston, M. E., Campbell, A. P., Lix, B., Kay, C. M., Sykes, B. D., and Hodges, R. S. (1996) *Biochemistry 35*, 10041−10050.
24. Wendt, H., Leder, L., Harma, H., Jelesarov, I., Baici, A., and Bosshard, H. R. (1997) *Biochemistry 36*, 204−213.
25. Wendt, H., Berger, C., Baici, A., Thomas, R. M., and Bosshard, H. R. (1995) *Biochemistry 34*, 4097−4107.
26. Chen, Y. H., Yang, J. T., and Chau, K. H. (1974) *Biochemistry 13*, 3350.
27. Speh, S., and Elias, H. (1994) *J. Biol. Chem. 269*, 6370−6375.
28. Chapman, S. K., Sinclair-Day, J. D., Sykes, A. G., Tam, S. C., and Williams, R. J. P. (1983) *J. Chem. Soc. Chem. Commun.*, 1152−1154.
29. Wherland, S., and Gray, H. B. (1976) *Proc. Natl. Acad. Sci. U.S.A. 73*, 2950−2954.
30. Zhou, J. S., and Kostic, N. M. (1993) *Biochemistry 32*, 4539−4546.
31. Sutin, N. (1979) in *Tunneling in Biological Systems* (Chance, B., Devault, D. C., Frauenfelder, H., Marcus, R. A., Schrieffer, J. R., and Sutin, N., Eds.) pp 201−227, Academic Press, New York.
32. Marcus, R. A., and Sutin, N. (1985) *Biochim. Biophys. Acta 811*, 265−322.

BI011156U